Temperature dependence of surface stress across an order-disorder transition: $p(1 \times 2)$O/W(110)

N. Stojić,[1,2] T. O. Menteş,[3] N. Binggeli,[1,4] M. A. Niño,[3] A. Locatelli,[3] and E. Bauer[5]

[1]*Abdus Salam International Centre for Theoretical Physics, Strada Costiera 11, Trieste 34151, Italy*
[2] *INFM-CNR Democritos, Theory @ Elettra group, Trieste, I-34151, Italy*
[3]*Sincrotrone Trieste S.C.p.A., Basovizza-Trieste 34012, Italy*
[4] *INFM-CNR Democritos, Trieste, I-34151, Italy*
[5]*Department of Physics, Arizona State University, Tempe, Arizona 85287-1504*

(Dated: March 22, 2010)

Strain relaxations of a $p(1 \times 2)$ ordered oxygen layer on W(110) are measured as a function of temperature across the disordering transition using low-energy electron diffraction. The measured strains approach values of 0.027 in the $[1\bar{1}0]$ and -0.053 in the [001] direction. On the basis of the measured strain relaxations, we give quantitative information on temperature-dependent surface stress using the results of *ab initio* calculations. From the surface formation energy for different strains, determined by first-principles calculations, we estimate that surface stress changes from -1.1 for the ordered phase to -0.2 N/m for the disordered one along $[1\bar{1}0]$, and from 5.1 to 3.4 N/m along [001]. Moreover, our observation that the strains scale inversely with domain size confirms that the strain relaxation takes place at the domain boundaries.

I. INTRODUCTION

Surface stress is a quantity important for the understanding of surface processes like reconstruction, interfacial mixing, segregation, critical film thickness and self-organization at solid surfaces.[1–5] Regarding the latter, recent studies have demonstrated that the stress-induced patterns occurring at the mesoscopic scale on metal and semiconductor surfaces[6–8] show a strong dependence on temperature,[9] suggesting that the change of surface stress with temperature can play a major role in determining their properties. In spite of the wide interest in these and other stress-driven phenomena, there are very few studies concerning the temperature dependence of surface stress.[10]

On the theoretical side, density-functional theory (DFT) is probably the most accurate method to study surface elastic properties; however its results apply to 0 K.[11] Non-zero temperatures can be investigated using model potentials and atomistic simulations, but in the literature there are few examples applied to surface elasticity as a function of temperatures.[12] More studies can be found on a related quantity, the surface free energy,[13–15] which, however, does not give information on surface stresses without knowledge of its dependence on the surface strain. On the experimental side, the crystal-bending method was used to measure stress changes due to adsorbed species at different temperatures.[16] Indirectly connected to surface stress, there are some measurements of temperature-dependent strain using x-ray diffraction. However, a truly temperature-dependent study of a given system is still lacking.

Here, we aim at estimating surface stress change as a function of temperature across the order-disorder transition of the $p(1 \times 2)$-O/W(110) structure, using an alternative approach which combines low-energy electron diffraction (LEED) and *ab initio* calculations. In addition to thermal expansion, the presence of the disordering is crucial in determining the surface stress changes, similar to the phenomenon of surface melting.[12] This stress change is also of particular importance for the recently reported high-temperature stress-induced pattern formation of Pd on W[9], due to the profound effect of O adsorption on the anisotropy of Pd stripes.[17]

Oxygen on W(110) is a well-studied model system characterized by a series of ordered phases as a function of oxygen coverage.[18,19] At 0.5 ML coverage O is ordered in a (1×2) structure, which consists of doubly-spaced close-packed rows of O in the $\langle\bar{1}11\rangle$ directions. The (1×2) phase contains eight equivalent domains generated by translations and rotation (by 109.5°) of the O lattice on the triply coordinated adsorption sites.[19] The $p(1 \times 2)$ O domains disorder at about 700 K. Bucholz and Lagally[20] describe the disordering by shrinking of the ordered domains with increasing temperature. At the same time, the surface stress is expected to be relieved at the domain boundaries.[19]

In this paper, we use LEED to detect the temperature-induced lattice changes in the O adlayer on W, and DFT calculations for their quantitative analysis in terms of surface stress. More precisely, we estimate the surface stress by using surface formation energy as a function of strain, calculated from first principles. We evaluate the surface stress at the values of strain for which the surface layer is found to be maximally relaxed (well above the disordering temperature). We focus on the behavior in a wide temperature range, and we show that the average change in atomic spacing of the surface layer for increasing temperature is a direct consequence of stress relaxation due to disorder on the surface. The analysis of lattice changes measured by LEED is done in the same way as in Ref. 21. Kinematic low energy electron diffraction, although similar to x-ray diffraction in the information sought, has the advantage of being inherently surface sensitive, even more so in the case of O/W(110)

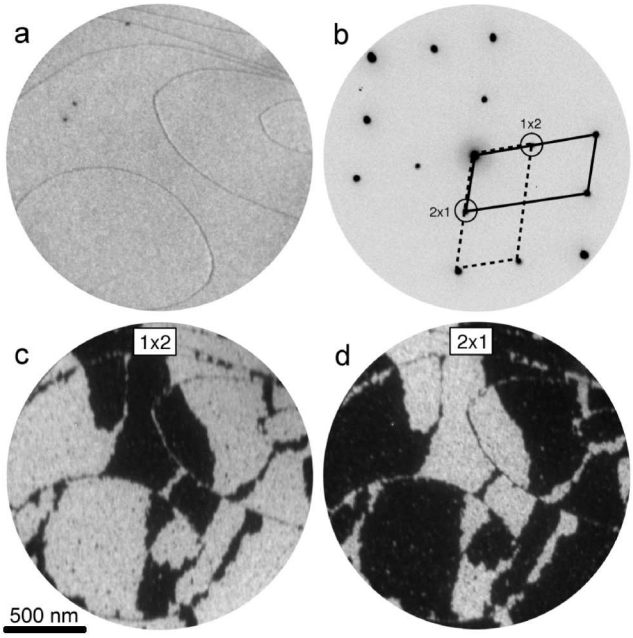

FIG. 1: (a) LEEM image of the partially (1x2) oxygen-covered W(110). Image diameter is 2 microns. The curved lines correspond to W atomic steps. (b) LEED pattern acquired from a 2 micron region at 35 eV electron energy. (c) and (d) Dark field LEEM images of the same region acquired using the half-order spots marked in panel (b). The bright/dark contrast corresponds to the 1×2 and 2×1 domains.

with the presence of half-order diffraction spots.

The paper is organized as follows: in section II we present the measured strain relaxations as a function of temperature, obtained by LEED. Section III summarizes our *ab initio* calculations of surface formation energy as a function of strain. Combining the two, we extract estimates of surface stress at high temperature, which is discussed in section IV. Conclusions are given in section V.

II. EXPERIMENTAL RESULTS

The LEED measurements were made with the spectroscopic photo-emission and low energy electron microscope SPELEEM at Elettra (Italy).[22] The instrument is a hybrid electron/x-ray microscope, which allows chemical and structural imaging combined with micro-spot LEED (μ-LEED).[22,23] In the latter mode, a LEED pattern was obtained from a region of 2 μm diameter. The transfer width of μ-LEED was determined to be 10 nm from measurements on a step-free region of the clean W(110) surface.

Cleaning of the W(110) single crystal was carried out by annealing at 1400 K in 2×10^{-6} mbar oxygen, followed by high temperature flashes in ultrahigh vacuum to remove oxygen. The surface cleanliness was confirmed by the absence of tungsten carbide islands and a sharp (1×1) LEED pattern. Using low-energy electron microscopy (LEEM), regions with micron-sized terraces were chosen in order to exclude broadening of diffraction spots due to the presence of step bunches.

The (1×2)-ordered 0.5 ML oxygen-covered surface was prepared by exposing the clean W(110) surface to molecular oxygen at 450 K. 0.5 ML coverage was assigned to the maximum intensity of the (1×2) diffraction spots, which was obtained at an exposure of about 4.6 Langmuirs.[21] After O exposure, we performed a short annealing at 1400 K under ultra-high vacuum conditions, which resulted in large domains with a sharp LEED pattern.

Figure 1a shows a LEEM image of the (1×2)-O/W(110) surface acquired below the disordering of oxygen, at around 400 K. The corresponding μ-LEED pattern is displayed in Fig. 1b. The very large (1×2) and (2×1) domains are visible in the *dark field* images shown in Fig. 1c and 1d.[24] The domain sizes reach micron scale with boundaries consisting of narrow regions with opposite domain orientation between two rotational domains showing no obvious directional anisotropy.

It should be noted that the presence or absence of translational domain boundaries within a region of single orientation (1×2 or 2×1) cannot be concluded from the images displayed in Fig. 1. However, the high intensity of the half-order diffraction spots confirms the presence of extended single domains. Nevertheless, fine lines and granularity in a single rotational domain in the high resolution images could point to the presence of defects (translational domain boundaries, oxygen vacancies, etc) within an otherwise perfect oxygen lattice.

This surface is used to monitor the strain relaxations at high temperature. The disordering of the (1×2) order as a function of temperature can be followed via the intensity and width of the half-order diffraction spots displayed in Fig. 2a. The decrease of intensity and the increase of spot widths are documented in the early literature[20,25] and can be understood as large domains breaking up into smaller ones with increasing temperature. This is also reflected in the shape of the diffraction spot profiles, which transforms from Gaussian to Lorentzian at about 600 K. Importantly, diffuse half-order spots can still be discerned up to above 1100 K. This means that the O atoms preserve the local (1×2) order (in small clusters) even though the long-range order is lost at high temperature.

In addition to the intensity and width, we can also measure the half-order peak positions as a function of temperature. The reciprocal lattice distances allow us to evaluate the *average* distance of O atoms within the (1×2)-ordered regions. The data analysis is carried out in the same way as in Ref. 21. The resulting strains, defined with respect to the underlying W lattice, in the two crystallographic directions are displayed in Fig. 2b. Clearly, the (1×2) O unit cell, which respects the W periodicity at low temperatures, on average expands along $[1\bar{1}0]$ and

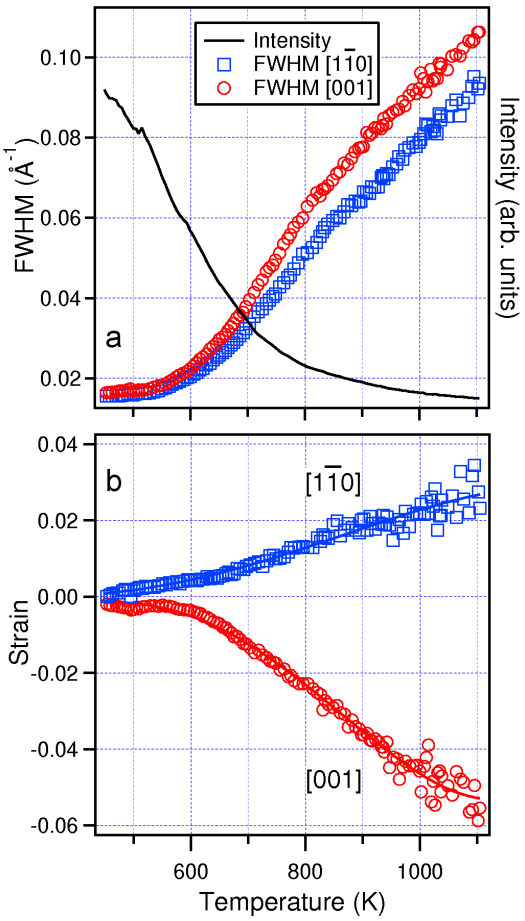

FIG. 2: (a) Peak intensity (solid line) and width of the half-order diffraction spots, measured at electron energy of 28 eV. (b) Measured strain, derived from the reciprocal distances of the half-order peak positions, as a function of temperature along two directions. Solid lines are the least-squares fit, indicated to guide the eye.

shrinks along [001] as the temperature increases and disorder sets in. At the highest temperatures the measured strains tend to reach values of about $\epsilon_{\rm relaxed} = 0.027$ in [1$\bar{1}$0] and $\epsilon_{\rm relaxed} = -0.053$ in [001] directions at 1100 K.

The measured values of the strain relaxation include a contribution from the thermal expansion of the W crystal. However, within the temperature range of interest, the change in lattice spacing due to this effect is less than 0.4 %,[26] which is comparable to the smallest measured surface strains.

Interestingly, the strains in both directions scale as inverse power laws of the average domain size as shown in Fig. 3. Domain sizes were extracted from the FWHM of half-order diffraction spots as displayed in Fig. 1a taking proper account of the instrumental broadening. The fit functions in the log-log plots in Fig. 3 are described by $\varepsilon \propto L^p$, and correspond to powers of $p = -1.09$ and -1.45 for [1$\bar{1}$0] and [001] directions, respectively. This observation is in line with the strain relaxations taking place at the domain boundaries. Moreover, the changes in strain as a function of O coverage at fixed temperature (450 K) are also included in Fig. 3 for comparison.[21] The important differences will be discussed in the following sections.

Note that the two main sources of error in the experiments are the limited instrument transfer width and the changes in the angular alignment as a function of temperature. The former makes the determination of domain sizes very difficult when the domains are larger than the transfer width (hence the broadening of the diffraction spots is dominated by the instrument function). However, considering that the transfer width is about 10 nm, this should be a negligible effect within the range displayed in Fig. 3. On the other hand, variations in angular alignment may introduce a small uncertainty in the spot positions, which might translate into slight deviations from the power law behavior. In order to reduce the possibility of such an artifact, we have averaged over equivalent lattice vectors in obtaining the reported strains.

III. *AB INITIO* CALCULATIONS

In this study, we use *ab initio* calculations to determine the surface formation energy, γ, for different strains. The strain derivative is used to evaluate the surface stress at the measured maximally-relaxed strain $\epsilon_{relaxed}$ of the O layer.

To calculate γ we perform DFT pseudopotential calculations in a plane-wave basis by using the `PWscf` code.[27] The local-density approximation (LDA) in the Perdew-Zunger parametrization[28] is used for the exchange and correlation functional. We utilize a symmetric slab with 11 layers to simulate the O/W system, with 9 vacuum layers. We employ Vanderbilt ultra-soft pseudopotentials,[29] generated using the $2s^2 2p^4$ atomic configuration of O and the $5s^2 5p^6 5d^4 6s^2$ configuration of W. The core-cutoff radii for O were: $r_{s,p} = 1.6$, $r_d = 1.4$ a.u. and for W: $r_{s,p} = 2.2$, $r_d = 2.4$ a.u. We use the equilibrium W bulk lattice constant of 3.14 Å. Our plane-wave-basis kinetic-energy cutoff is 35 Ry for the wave functions and 350 Ry for the charge density. We use a $26 \times 13 \times 1$ Monkhorst-Pack[30] mesh for the k-points sampling in the Brillouin zone of the (1×2) surface.

γ is evaluated from the expression:

$$\gamma = \frac{1}{2A}(E_{\rm slab} - N_W E_W^B - \frac{N_O}{2} E_{O_2}), \qquad (1)$$

where A is the strain-dependent surface area, $E_{\rm slab}$ stands for the total energy of the whole slab, N_W for the number of W atoms, E_W^B for the W bulk energy per atom, N_O for the number of O atoms and E_{O_2}[31] is the energy of the O_2 molecule. E_{slab} is evaluated for several different homogeneous uniaxial [1$\bar{1}$0] and [001] strains on the slab and E_W^B is recalculated for each strain. We note

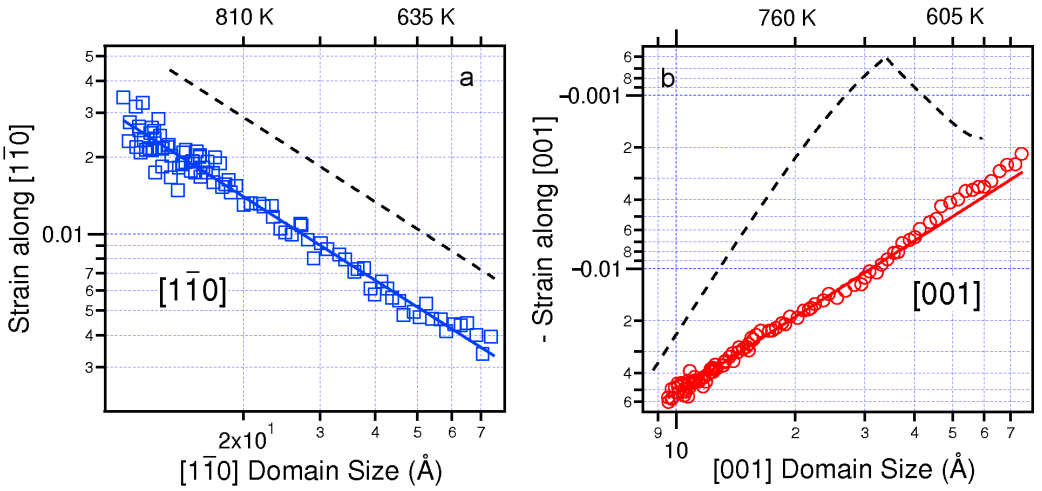

FIG. 3: Changes of strain along (a) [1$\bar{1}$0] and (b) [001] as a function of the average dimension of the (1 × 2) domains. The squares and circles are the data extracted from the LEED measurements, while the solid lines are fits to the power-law functions. Temperatures corresponding to 20, 50 and 100 Å domain sizes are noted above. Strains obtained in Ref. 21 as a function of oxygen coverage at fixed temperature are included as dashed lines for comparison.

that the constant energy E_{O_2} does not contribute to the derivative of energy and, therefore, is not relevant to the discussion of surface stress.

On the basis of the calculated γ for various strains and a fitted polynomial curve, the surface stress, τ_i,[32] is obtained by using:[33]

$$\tau_i = \frac{1}{A}\frac{\partial(A\gamma)}{\partial\epsilon_i}, \qquad i = 1, 2 \tag{2}$$

where ϵ_i is the uniaxial strain. Figure 4 presents γ multiplied by the area[34] for a few strains, as well as polynomial fits to the calculated points for both directions. We assume that the two directions can be considered independently. In the [1$\bar{1}$0] direction, a quadratic function fits the data very well, while for the [001] direction, due to higher-order terms, a better fit is obtained by a cubic polynomial.

Calculated values of τ are presented in Table I. In the first column are our $p(1\times2)$O/W(110) surface stress values calculated from the curves in Fig. 4 at $\epsilon = 0$. The second column contains the same quantities, for comparison, from Ref. 21 (calculated with the expression derived by Nielsen and Martin[35] for the stress tensor σ based on the Hellmann-Feynman theorem) for both directions. Finally, in the last column are our estimates for the average surface stress in the high-temperature phase, with no long-range order ($\tau_{\mathrm{disO}(1\times2)}$), as obtained from the derivative of the energy curve in Fig. 4 at $\epsilon_{\mathrm{relaxed}}$.

direction	$\tau^{\gamma}_{\mathrm{O}(1\times2)}$	$^{a}\tau_{\mathrm{O}(1\times2)}$	$\tau^{\gamma}_{\mathrm{disO}(1\times2)}$ at $\epsilon_{\mathrm{relaxed}}$
[1$\bar{1}$0]	−1.1	−1.1	−0.2
[001]	5.1	5.4	3.4

^{a}Ref. 21

TABLE I: Surface stresses at $\epsilon = 0$ calculated from the γ curve (first column) and by a direct DFT surface stress calculation[21] (second column). Last column contains surface stresses at $\epsilon_{\mathrm{relaxed}}$, estimated from the γ curve. The values are given in N/m. The positive sign corresponds to the tensile stress.

IV. DISCUSSION

The calculated values in Table I for the stresses at $\epsilon = 0$ using the two approaches, from the γ curve and by a direct DFT calculation of the surface stress, give similar results in both directions. The differences are within the estimated error, 0.35 N/m,[21] of the calculated surface stress and the propagated error of the fitting parameters of ∼ 0.20 N/m. The different slab thicknesses in the two calculations (15 layers for the direct stress calculation and 11 layers for the total energy calculation of the strained slabs) also may contribute to the difference. The surface stress values at $\epsilon_{\mathrm{relaxed}}$ (high-temperature phase) indicate a significant reduction with respect to the values at $\epsilon = 0$ (0 K).

To better understand the physical significance of the values listed in the last column in Table I, we need to describe the underlying assumptions. Most importantly, we assume that the disordering takes place predominantly within the O layer and that the temperature changes in stress are mostly due to this disorder. The basis for the first approximation is that W atoms do not participate in the (1 × 2) order to begin with.[36–38] Therefore, they

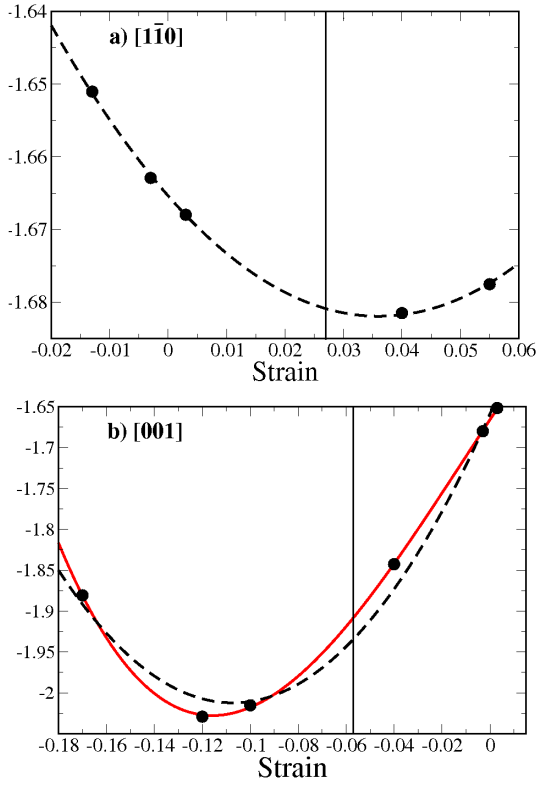

FIG. 4: *Ab initio* calculations of the surface formation energy multiplied by the surface unit cell area as a function of strain in a) [1$\bar{1}$0] and b) [001] directions. Black dashed curves show quadratic fit, while the solid red line is for a cubic fit. Full circles indicate calculated points. The vertical line corresponds to the measured strain, $\epsilon_{relaxed}$, of the O layer at high temperature.

are expected to be disturbed little by the disordering of the O lattice, if at all. The second assumption is based on the small effect of the bulk thermal expansion of W.

As we noted in the introduction, with increasing temperature, the O lattice loses long-range order by breaking of large domains into smaller ones. It is expected that the loss of order should result in a reduction of stress within the O layer with the stress relieved at the domain boundaries.[19] In the limiting case of complete disorder (a dense gas of O atoms) one would expect negligible stress in the O layer, and the remaining surface stress would be mostly dominated by the underlying W layer. On the other hand, the presence of the half-order diffraction spots at the highest temperatures measured, however weak and diffuse, suggests that the O layer has still short-range order. Therefore, the high temperature surface stress can be decomposed into contributions from the unmodified W layers and from the *partially relaxed* oxygen surface.

In order to represent this situation, in our theoretical analysis, ideally, we would like to calculate stresses for the strains within the oxygen layer equal to ϵ_{relax} and keeping the bulk unstrained in the same slab. However, such inhomogeneous strain is not affordable in our supercell calculations. Therefore, we use slabs in which both the bulk and the surface part are strained to $\epsilon_{relaxed}$ (with subsequent subtraction of the bulk contributions). To see how this theoretical treatment corresponds to the experiment in which we measure only the surface-layer strain with W underneath at its equilibrium lattice constant (strain zero), we examine the layer-resolved stresses as a function of strain. From Eq. 1 and 2, the uniaxial surface stress can be written as:

$$\begin{aligned}\tau_i(\epsilon_i) &= \tfrac{1}{2}\tfrac{V}{A}[\sigma_{\mathrm{i,slab}}(\epsilon_i) - N_W\sigma^{\mathrm{B}}_{\mathrm{i,W}}(\epsilon_i)] \\ &= \tfrac{1}{2}\tfrac{V}{A}[\sigma_{\mathrm{i,surf}}(\epsilon_i) + \sigma_{\mathrm{i,subsurf}}(\epsilon_i) + (N_W-1)\sigma^{\mathrm{B}}_{i,W}(\epsilon_i) \\ &\quad -N_W\sigma^{\mathrm{B}}_{\mathrm{i,W}}(\epsilon_i)],\end{aligned} \tag{3}$$

where $\sigma_{\mathrm{i,slab}}(\epsilon_i) = (1/V)\partial E_{\mathrm{slab}}(\epsilon_i)/\partial\epsilon_i$ and $\sigma^{\mathrm{B}}_{\mathrm{i,W}}(\epsilon_i) = (1/V)\partial E^{\mathrm{B}}_{\mathrm{W}}(\epsilon_i)/\partial\epsilon_i$ are the volume-averaged stresses, V is the volume of the unit cell and the indices "surf" and "subsurf" stand for the surface O and the subsurface W layers, respectively. Assuming that the subsurface layer's proximity to the surface changes its stress-strain relation only by addition of a constant stress (which corresponds to the stress at zero strain, see the Appendix), with respect to the bulk, we are left with:

$$\tau_i = \frac{1}{2}\frac{V}{A}\left[\sigma_{\mathrm{i,surf}}(\epsilon_i) + \sigma_{\mathrm{i,subsurf}}(\epsilon=0)\right]. \tag{4}$$

Under the above assumption, our calculated stress at $\epsilon_{\mathrm{relaxed}}$ has two contributions: from the surface O layer at $\epsilon_{\mathrm{relaxed}}$ and from the W subsurface layers at the strain zero.[39] We note that our assumption for Eq. 4 is analogous to saying that the elastic constants of the subsurface and bulk layers are identical. A heuristic interpretation of Eq. 3 and 4 can be found in the Appendix.

A confirmation that the elastic response of the subsurface W is close to that of bulk W is obtained by inspecting the relaxed positions in our calculated O/W slab. We find that the average interlayer spacing of the two topmost W layers below O is very close to its bulk value ($\Delta d_{23} = -1.1$ %), while the clean W surface relaxes by $\Delta d_{12} = -3.6$ %.[21] This indicates that the W surface when covered with O becomes much more bulk-like. We note that our results for Δd_{23} for O/W and Δd_{12} for W agree well with other theoretical results, $\Delta d_{23} = -1.3$ % (Ref. 40) for the former and $\Delta d_{12} = -3.6$ % (Ref. 41) for the latter case. Experimentally, $\Delta d_{12} = -3.1$ % for W.[41]

In spite of the assumptions mentioned above, there are important conclusions to draw from the results. Interestingly, our results in Table I show that the surface stress and its anisotropy do not vanish even several hundred degrees above the disordering transition at about 600 K. This is mainly due to short-range correlations within the

O layer persisting at high temperatures. The other contribution, which may be equally significant, is the nonzero stress within the subsurface layers which do not participate in the disordering. A discrimination of the two effects needs a layer-resolved stress calculation, which is beyond the scope of our study.

Another point is the confirmation that stress is relieved at the domain boundaries, which is derived from the power-law behavior in Fig. 3. Although this is qualitatively similar to the relaxations at the boundaries of small $p(1\times2)$O islands on W(110),[21] there are differences to be emphasized. The strain relaxation at the boundary between two distinct phases is driven by the difference in surface stress, as shown in Ref. 21. However, in the case of the fully O-covered surface, the mechanism of the stress relaxation is somewhat different.

To verify that, we constructed heavy and light domain-wall configurations and compared their energy on the basis of broken and newly-formed bonds, using the lateral interaction parameters for up to the third neighbors.[42] This simple analysis yields a vacancy line (light-domain wall between the (1x2) and (2x1) domains) as the most favorable domain-wall configuration for the main crystallographic directions on W(110). Although the energy difference between this and some heavier domain walls is smaller than 10 meV/Å, this estimate does not include the energy obtained by strain relaxations, which is the largest for this type of the boundary, as it allows the largest atomic relaxations. Predominant vacancy-type domain walls would, indeed, confirm the view that the stress is relaxed at the domain boundaries in this system.

The differences between strain relaxation at an *island boundary* and a *domain boundary* are underlined in Fig. 3. Most importantly, i) along $[1\bar{1}0]$ strain relaxation on fully oxygen-covered surface as a function of domain size with increasing temperature shows a considerably reduced magnitude (but identical slope) compared to that of relaxation for small oxygen islands as a function of island size with increasing coverage at fixed temperature (dashed line in Fig. 3a), ii) along [001] both magnitude and slope of the strain curves are drastically different between two data sets. From the first point we conclude that along $[1\bar{1}0]$ the force driving the strain relaxation at the boundary is reduced for the fully O-covered surface, however the relaxation mechanism remains the same. The island boundary responds to the stress difference between O-covered and clean tungsten, which is -4.7 N/m.[21] This is, indeed, considerably larger than the stress on fully O-covered surface along $[1\bar{1}0]$ (see Table I) and it points to the idea that at the domain boundaries the relaxation is driven by the stress itself and not a difference of stresses. The comparison along [001] gives an even stronger support to this discussion. In the case of an O island, the boundary almost feels no force along [001] and therefore the relaxation is a higher-order effect decaying rapidly with increasing island size (dashed line in Fig. 3b). However, in the fully O-covered surface the strain scales with a power of domain size much closer to a $1/L$ power law, which is similar to the behavior along $[1\bar{1}0]$. This is in line with the idea that the domain boundary is relaxing under the influence of the large tensile stress along [001].

We emphasize that an anisotropic thermal expansion of the oxygen layer cannot replace surface stress as the driving force of the observed strain relaxations. This is clearly shown in the size of the oxygen unit cell as a function of temperature, which can be derived from the data in Fig. 2. The oxygen unit mesh expands slightly from 400 K to 600 K, above which it contracts almost linearly with increasing temperature. The contraction is explained by the predominantly tensile stress within the oxygen layer.

Having shown qualitatively that the strain relaxations are due to the stress itself and not the stress difference, we note that also the sign of the measured strain relaxation in the two directions supports this conclusion, as well as the ratio of the strain relaxations (large response in the direction of larger surface stress). However, it is interesting to observe that the strain relaxation along $[1\bar{1}0]$ is only two times smaller than along [001], and not five times, as could be expected from the stress ratio in the two directions. This is explained by different potential profiles in the two directions, according to which O atoms move much easier along $[1\bar{1}0]$, than [001].[43]

V. CONCLUSION

In this work, we have measured the strain relaxation as a function of temperature across the disordering transition of $p(1\times2)$O/W(110). The breaking up of large domains into smaller ones as a function of temperature can be observed by the changes of the intensity and width of the half-order diffraction spots. Following the changes of the spot distances we extracted the strain relaxation as a function of temperature. At T$\sim$ 1100 K the measured strains reach values of 0.027 along $[1\bar{1}0]$ and -0.053 along [001]. We found that the measured stresses are roughly proportional to the inverse domain size. By means of *ab initio* calculations, we determined the surface formation energy as a function of strain, from which we estimated the surface stress values at the measured relaxed strains.

VI. APPENDIX

In order to give a heuristic interpretation of Eq. 3 and 4 in terms of energy, in Fig. 5 we show the slab energy decomposed in layers[44] as a function of strain. Horizontal and vertical axes represent strain and energy, respectively. The layer-energy dependence is shown shifted in energy, for ease of viewing. The top parabola corresponds to the O surface, while those below stand for the subsurface and bulk W layers from top to bottom. For simplic-

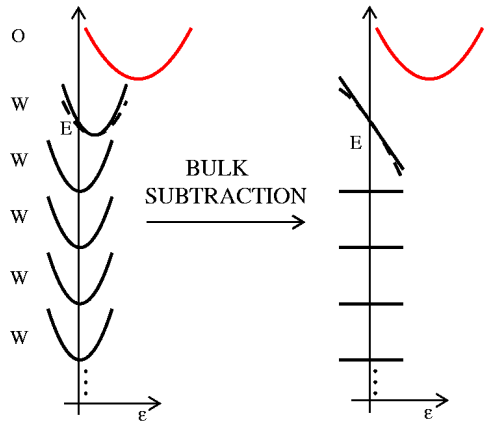

FIG. 5: A schematic of energy decomposition in layers before (left) and after the subtraction of the bulk energy (right). Red curve represents O surface, and the full black line stands for the W layers. The dashed line in the second layer from the top represents a case with slightly changed curvature of the W parabola. Dots indicate continuation of bulk layers, while flat lines describe zero energy contribution. The horizontal axis represents strain and the vertical axis stands for energy (contributions from different layers are drawn with energy shift).

ity, only the O and the subsurface W layers are shown to be modified with respect to bulk W. This decomposition is the energy analog of Eq. 3. For the subsurface W we show two curves, one identical to the bulk curves, and the other one with 25 % smaller curvature.

When we subtract, as is done to determine surface formation energy, the bulk W energy from all the W layers, we are left with only two non-zero contributions, from the surface and subsurface layers, as shown on the right side of the figure. In the case when the subsurface parabola is identical to the bulk one, the remaining contribution after subtraction to the surface energy is a line, which will give a constant stress for all strains, as written in Eq. 4. For a subsurface parabola slightly different from the bulk one, the resulting contribution to the surface formation energy has a very small curvature, yielding a slowly-varying stress as a function of strain.

Finally, adding the energy of the subsurface layer to the surface-layer parabola, we obtain a curve comparable to Fig. 4, which corresponds to the surface stress of the O layer and also contains contribution from the W subsurface layer at strain zero.

Acknowledgments

We acknowledge support for this work by the INFM-CNR and CINECA within the framework "Iniziativa Calcolo per la Fisica della Materia".

[1] W. Haiss, Rep. Prog. Phys. **64**, 591 (2001).
[2] H. Ibach, Surf. Sci. Rep. **29**, 195 (1997).
[3] S. Narasimhan and D. Vanderbilt, Phys. Rev. Lett. **69**, 1564 (1992).
[4] L. P. Nielsen, F. Besenbacher, I. Stensgaard, E. Laegsgaard, C. Engdahl, P. Stoltze, and J. K. Norskov, Phys. Rev. Lett. **74**, 1159 (1995).
[5] R. C. Cammarata and K. Sieradzki, Annu. Rev. Mater. Sci. **24**, 215 (1994).
[6] D. E. Jones, J. P. Pelz, Y. Hong, E. Bauer, and I. S. T. Tsong, Phys. Rev. Lett. **77**, 330 (1996).
[7] K. Kern, H. Niehus, A. Schatz, P. Zeppenfeld, J. Goerge, and G. Comsa, Phys. Rev. Lett. **67**, 855 (1991).
[8] R. van Gastel, R. Plass, N. C. Bartelt, and G. L. Kellogg, Phys. Rev. Lett. **91**, 055503 (2003).
[9] T. O. Menteş, A. Locatelli, L. Aballe, and E. Bauer, Phys. Rev. Lett. **101**, 085701 (2008).
[10] A. T. N'Diaye, R. van Gastel, A. J. martinez Galera, J. Coraux, H. Hattab, D. Wall, F.-J. M. zu Heringdorf, M. H. von Hoegen, J. M. Gomez-Rodriguez, B. Poelsema, et al., New J. Phys. **11**, 113056 (2009).
[11] Disordered systems, for example, can be dealt with using DFT in a straighforward manner, but at a price of creating very large supercells and various configurations which are to be averaged. This is often impractical or impossible due to limited computer resources.
[12] T. Frolov and Y. Mishin, Phys. Rev. B **79**, 045430 (2009).
[13] J. S. Vermaak and D. K. Wilsdorf, J. Phys. Chem. **72**, 4150 (1968).
[14] S. M. Foiles, Phys. Rev. B **49**, 14930 (1994).
[15] J. Q. Broughton and G. H. Gilmer, Acta Metall. **31**, 845 (1983).
[16] A. Grossmann, W. Erley, and H. Ibach, Surf. Sci. **337**, 183 (1995).
[17] T. O. Menteş *et al*, in preparation.
[18] G.-C. Wang, T.-M. Lu, and M. G. Lagaly, J. Chem. Phys. **69**, 479 (1978).
[19] K. E. Johnson, R. J. Wilson, and S. Chiang, Phys. Rev. Lett. **71**, 1055 (1993).
[20] J. C. Buchholz and M. G. Lagally, Phys. Rev. Lett. **35**, 442 (1975).
[21] T. O. Menteş, N. Stojić, N. Binggeli, M. A. Niño, A. Locatelli, L. Aballe, M. Kiskinova, and E. Bauer, Phys. Rev. B **77**, 155414 (2008).
[22] A. Locatelli, L. Aballe, T. O. Menteş, M. Kiskinova, and E. Bauer, Surf. Interface Anal. **38**, 1554 (2006).
[23] E. Bauer, Rep. Prog. Phys. **57**, 895 (1994); P. Hawkes and J. Spence, *Science of Microscopy* (Springer, New York, 2007), pp. 606-656.
[24] A *dark field* image is obtained with electrons that give rise to a particular diffraction spot, which are selected by an aperture placed in the back-focal plane of the microscope.
[25] T. Engel, H. Niehus, and E. Bauer, Surf. Sci. **52**, 237 (1975).

[26] *American Institute of Physics Handbook*, edited by D. E. Gray (McGraw-Hill Book Company, New York, 1972); A. G. Worthing, Phys. Rev. **10**, 638 (1917).

[27] P. Giannozzi, S. Baroni, N. Bonini, M. Calandra, R. Car, C. Cavazzoni, D. Ceresoli, G. L. Chiarotti, M. Cococcioni, I. Dabo, et al., J. Phys.: Condens. Matter **21**, 395502 (2009).

[28] J. P. Perdew and A. Zunger, Phys. Rev. B **23**, 5048 (1981).

[29] D. Vanderbilt, Phys. Rev. B **41**, 7892 (1990).

[30] H. J. Monkhorst and J. D. Pack, Phys. Rev. B **13**, 5188 (1976).

[31] E_{O_2} is calculated for an isolated, spin-polarized molecule in a large supercell.

[32] We write all equations for the case of uniaxial stress, which we use for our analysis, but the general tensor stress components, $\tau_{i,j}$ can be used in the same expressions in place of uniaxial stresses. We note that our calculations gave us non-diagonal stresses always smaller than 10 % of the value of the diagonal terms.

[33] R. Shuttleworth, Proc. Phys. Soc. London Sect. A **63**, 444 (1950).

[34] In our calculational cell, $A = 13.94$ $\mathring{A}^2$ at the equilibrium lattice constant.

[35] O. H. Nielsen and R. M. Martin, Phys. Rev. Lett. **50**, 697 (1983).

[36] M. A. V. Hove and S. Y. Tong, Phys. Rev. Lett. **35**, 1092 (1975).

[37] R. X. Ynzunza, R. Denecke, F. J. Palomares, J. Morais, E. D. Tober, Z. Wang, F. J. G. de Abajo, J. Liesegang, Z. Hussain, M. A. V. Hove, et al., Surf. Sci. **459**, 69 (2000).

[38] Our previous DFT results[21] indicate that the W atomic positions are only slightly modified upon O adsorption, both laterally and along the surface normal.

[39] In Eq. 3 we could have chosen any number of subsurface layers to be considered separately. They would all give a contribution to the surface stress in Eq. 4 at the zero strain.

[40] M. Stöhr, R. Podloucky, and S. Muller, J. Phys. Cond. Matter **21**, 134017 (2009).

[41] M. Arnold, G. Hupfauer, P. Bayer, L. Hammer, K. Heinz, B. Kohler, and M. Scheffler, Surf. Sci. **382**, 288 (1997).

[42] P. K. Wu, M. C. Tringides, and M. G. Lagally, Phys. Rev. B 39, 7595 (1989); C. Uebing and R. Gomer, Surf. Sci. 381, 33 (1997); M. A. Zaluska-Kotur, A. Lusakowski, S.Krukowski, and L. A. Turski, Surf. Sci. 566-568, 210 (2004).

[43] M. A. Załuska-Kotur, S. Krukowski, Z. Romanowski, and Ł. A.. Turski, Phys. Rev. B **65**, 045404 (2001).

[44] Chetty and Martin developed a formalism for calculations of energy density in DFT [N. Chetty and R. Martin, Phys. Rev. B **45**, 6074 (1992)], which can be used for layer-resolved energy calculations, and, based on the same formalism, also stress density can be calculated [A. Filippetti and V. Fiorentini, Phys. Rev. B **61**, 8433 (2000)].